ELSEVIER

Contents lists available at ScienceDirect

Analytical Biochemistry

journal homepage: www.elsevier.com/locate/yabio



Solid phase synthesis and spectroscopic characterization of the active and inactive forms of bacteriophage S²¹ pinholin protein



Daniel L. Drew Jr., Tanbir Ahammad, Rachel A. Serafin, Brandon J. Butcher, Katherine R. Clowes, Zachary Drake, Indra D. Sahu, Robert M. McCarrick, Gary A. Lorigan*

Department of Chemistry and Biochemistry, Miami University, Oxford, OH, 45056, USA

ARTICLE INFO

Keywords:
Bacteriophage S21 pinholin
Solid phase peptide synthesis
Circular dichroism
Electron paramagnetic resonance spectroscopy
Solid state-NMR spectroscopy

ABSTRACT

The mechanism for the lysis pathway of double-stranded DNA bacteriophages involves a small hole-forming class of membrane proteins, the holins. This study focuses on a poorly characterized class of holins, the pinholin, of which the S^{21} protein of phage $\varphi 21$ is the prototype. Here we report the first in vitro synthesis of the wildtype form of the S^{21} pinholin, $S^{21}68$, and negative-dominant mutant form, $S^{21}IRS$, both prepared using solid phase peptide synthesis and studied using biophysical techniques. Both forms of the pinholin were labeled with a nitroxide spin label and successfully incorporated into both bicelles and multilamellar vesicles which are membrane mimetic systems. Circular dichroism revealed the two forms were both > 80% alpha helical, in agreement with the predictions based on the literature. The molar ellipticity ratio $[\theta]_{222}/[\theta]_{208}$ for both forms of the pinholin was 1.4, suggesting a coiled-coil tertiary structure in the bilayer consistent with the proposed oligomerization step in models for the mechanism of hole formation. ^{31}P solid-state NMR spectroscopic data on pinholin indicate a strong interaction of both forms of the pinholin with the membrane headgroups. The ^{31}P NMR data has an axially symmetric line shape which is consistent with lamellar phase proteoliposomes lipid mimetics.

1. Introduction

The final step of the double-stranded DNA bacteriophage infection cycle is host lysis [1–3]. The mechanism for this lysis pathway involves three proteins, a small hole-forming inner membrane protein known as the holin, a muralytic enzyme known as the endolysin, and the spanin complex responsible for outer membrane disruption [3,4]. The function of the holin protein is to permeabilize the inner phospholipid bilayer allowing the release of the endolysin to begin the degradation of the peptidoglycan [5]. This is accomplished by a harmless accumulation of the holin in the host cell membrane until the protein "triggers" at an allele-specific time. Triggering is the term used to denote when the holin reaches a critical concentration in the membrane and attains the functionality to permeabilize the membrane [3]. Due to the variation in mechanisms and sizes of lesions formed between different classes of holins the lesions have been termed "holes" to show distinction from channels and other such membrane permeabilization pathways [2,3].

Initially it was believed that all holins, like the λ S105 canonical holin, trigger to form micron-scale holes in the inner cell membrane [3]. These holes allowed for non-selective escape of fully folded and

functional endolysin enzymes. However, more recently a second type of holin has been discovered [2,6]. Instead of forming micron-scale nonselective holes in the cytoplasmic membrane, these holins form nanometer-scale holes that are only responsible for the depolarization of the membrane [2,6]. Due to the small size of the holes, this new class of holin was named the pinholin. Unlike the large hole forming canonical holins the hole created by the pinholins is not large enough to allow for the nonspecific escape of functional endolysin from the cytoplasm. Instead these pinholins are paired with signal-anchor-release (SAR) endolysins [2,3]. These proteins are named for a special N-terminal transmembrane helix that acts as an uncleaved signal sequence, resulting in a sec-mediated export. The SAR-endolysins accumulate in the periplasm as membrane-tethered, inactive enzymes. When the pinholins trigger and cause depolarization of the membrane, the SAR domain exits the bilayer, allowing the periplasmic catalytic domain to refold to its active form and begin degradation of the peptidoglycan [6-8].

This study focuses on the optimization of the solid phase peptide synthesis and spectroscopic characterization of the pinholin membrane protein system. More specifically, the system under study is encoded by the S^{21} holin gene of the lambdoid bacteriophage $\varphi 21$. The 71-codon

^{*} Corresponding author. Department of Chemistry and Biochemistry, 651 E. High St., Oxford, OH, 45056, USA. *E-mail address:* lorigag@miamioh.edu (G.A. Lorigan).

Active Pinholin S ²¹ 68	MĎK <u>ISTĠIAYĠŤSAGŚÂGYWFĹQWL</u> ďQVSPŠQ <u>WAAÍĠVLGŚĹVLGFĹTYLŤŇLYF</u> KĨREDŔŔKAARĠE TMD1 TMD2
Antiholin S ²¹ 71	<mark>MK</mark> SMĎK <u>ISTĠIAYĠŤSAGŚÄGYWŦĹQWL</u> ĎQVSPŠQ <u>WAATĠVLGŚĹVLGŦĹTYLŦŇLYF</u> KĨREDŔŔKAARĠE TMDI TMD2
Inactive Pinholin	$\begin{array}{c} \mathbf{M_{RYIRS}^{H}} \ddot{\mathbf{b}} \mathbf{K_{IST}^{G}} \mathbf{i} \mathbf{a} \mathbf{y} \mathbf{G^{T}SAGS^{G}AGYWF^{T}_{LQWL}} \mathbf{y} \mathbf{v} \mathbf{s} \mathbf{j} \mathbf{v} \mathbf{w} \mathbf{a} \mathbf{a} \mathbf{GV_{LGS^{T}_{L}VLGF^{T}_{L}VLT^{T}_{NLYF}}} \mathbf{v} \mathbf{v} \mathbf{s} \mathbf{e} \mathbf{v} \mathbf{v} \mathbf{v} \mathbf{e} \mathbf{v} \mathbf{v} \mathbf{v} \mathbf{v} \mathbf{v} \mathbf{v} \mathbf{v} v$

Fig. 1. This table shows the primary sequence for the active $S^{21}68$ form of pinholin, its cognate antiholin $S^{21}71$, and the inactive $S^{21}IRS$ form of the pinholin. Transmembrane domains (TMD) 1 and 2 are underlined with the spin labeled position highlighted in yellow. The three additional amino acids for the antiholin are shown in red with the positive charge responsible for timing denoted under the Lys. The IRS tag responsible for preventing TMD1 ex-

ternalization of S²¹68 is highlighted in red with the additional two positive charges denoted on the Arg residues. (For interpretation of the references to colour in this figure legend, the reader is referred to the Web version of this article.)

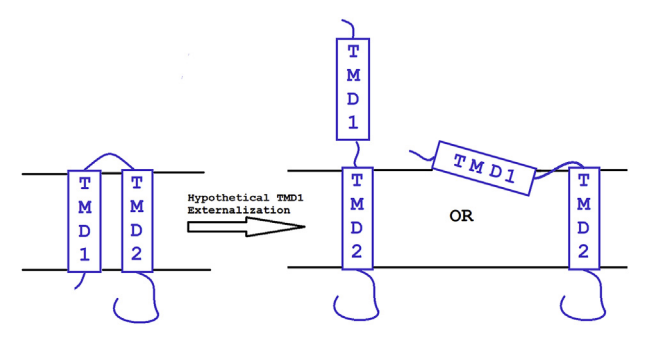


Fig. 2. The schematic shows the hypothetical pinholin TMD1 and TMD2 conformations in the membrane as well as possible TMD1 externalization orientations.

S²¹ gene has a dual translational start motif [9,10]. This results in the synthesis of two gene products, S²¹71 and S²¹68, resulting from translational initiations from codon Met1 and Met4, respectively. These two gene products are outlined in Fig. 1. The S²¹68 is the functional or active form of the pinholin. This form of pinholin has two transmembrane domains (TMDs), the first of which (TMD1) externalizes from the membrane, while the second (TMD2) remains embedded in the bilayer and is essential for lytic functionality [11-13]. The second form, $S^{21}71$, is known as the antiholin. The antiholin is responsible for the delayed triggering of the pinholin due to the addition of a positively charged lysine on the N-terminus (Fig. 1) which drastically slows the externalization of TMD1. A basic schematic for the orientation of the pinholin in the membrane as well as hypothetical conformations of externalized TMD1 can be seen in Fig. 2. The pinholin pathway begins with the accumulation of both forms of pinholin embedded in the bilayer, accumulating as dimers. Since the S²¹68/S²¹71 production ratio is ~2:1, the dimers are mostly S2168:S2168 homodimers and S²¹68:S²¹71 heterodimers [14]. Activation is thought to require externalization of TMD1 from the bilayer. Once both TMD1 segments are externalized, the pinholin dimer is licensed to continue in a pathway of oligomerization. When concentration of the activated pinholin dimers reach a critical concentration, the pinholin population triggers and causes massive and sudden depolarization of the inner cell membrane

The structure, mechanism, and model pathway of the pinholin protein has been difficult to study primarily because pinholin is not only a hydrophobic membrane protein but also expresses lethal in function, thus prohibiting high-level biosynthesis. The pinholin system poses an interesting challenge as the length of the pinholin and antiholin proteins are near the limit of solid phase peptide synthesis. The resulting function of the pinholin pathway is well known, but the individual steps of the dimerization and oligomerization in the pathway are not well studied. The Young group has shown that the addition of the five amino acid sequence 'RYIRS' to the N-terminus of the S²¹68 pinholin, shown in Fig. 1, prevents the externalization of TMD1 and ultimately the function of the pinholin pathway [12]. This is called the inactive IRS form of the pinholin. This presents an opportunity for recapitulating the holin pathway in vitro, using appropriate proportions of the wildtype pinholin (S²¹68) and the S²¹IRS, as a surrogate

antipinholin to control the pathway. Utilizing this control, the structure and dynamics of the pinholin protein as it progresses through the lytic pathway can be spectroscopically studied with a variety of biophysical techniques.

This study represents the first time that solid phase peptide synthesis has been used to study any holin system in vitro. Circular dichroism has been used to determine alpha helical protein secondary structure as well as probe the initial oligomerization steps required in the proposed pinholin lytic pathway. The extant biophysical information on the oligomerization of pinholin was conducted on a truncated version of the protein where only TMD2 was present [11,14]. However, this study uses the full length pinholin system. Electron paramagnetic resonance (EPR) spectroscopy was used to confirm pinholin incorporation into an in vitro multilamellar vesicle mimetic system. In conjunction with EPR spectroscopy, ³¹P solid-state NMR spectroscopy was used to discern the effect the different pinholin forms have on the membrane from the perspective of the phospholipids.

2. Material and methods

2.1. Solid phase peptide synthesis

The solid phase peptide synthesis of pinholin peptides was conducted using a CEM Liberty Blue Peptide Synthesizer with Discovery Bio Microwave System. The synthesis used a NovaSyn TG amino resin, a composite of low cross-linked polystyrene with the PEG chains terminally functionalized with an amino group. All syntheses were run at a 0.1 mM scale with Dimethylformamide (DMF) as the base solvent. All Fmoc protected amino acid solutions were prepared at a 0.2 M concentration and coupled using a standard activator and activator base pair of DIC and oxyma, respectively. The coupling reactions were run at 90 °C for 4 min while the Fmoc deprotection was run with 20% v/v piperidine in DMF at 93 °C for 1 min [16]. As seen in Fig. 1, the pinholin protein is naturally cys-less, requiring the introduction of only one site-specific cysteine into the primary sequence for site directed spin labeling EPR experiments.

2.2. Protecting group and solid phase cleavage

The solid phase bound pinholin peptide was washed three times with dichloromethane and allowed to dry on a vacuum filter. The amino acid side chain protecting groups as well as the solid phase resin were cleaved from the peptide in a three-hour Trifluoroacetic acid (TFA) cleavage reaction [17–19]. The cleavage solution was then gravity filtered to remove the cleaved solid phase resin. TFA was evaporated from the reaction solution using inert nitrogen gas flow. Tertbutyl ether was added in excess to precipitate the pinholin peptide and separate from the still solubilized protecting groups [16]. The precipitated peptide was centrifuged down into a pellet by spinning for 15 min at 9000 rpm and the excess ether was decanted off. This procedure was repeated three times to ensure that all the protecting groups and scavengers were removed. Following the three ether washes the pinholin peptide was placed in a vacuum desiccator to dry for at least 8 h.

2.3. Protein purification and spin labeling

The crude pinholin peptide was purified by reverse phase high pressure liquid chromatography (RP-HPLC) using a C4 column running a two-solvent gradient. The first solvent was deionized water, the second was 90% HPLC grade acetonitrile. Both solvents were degassed and then acidified with 0.1% TFA by volume. The pinholin peptide was collected in fractions and the molecular weight of the peptide was confirmed using Matrix Assisted Laser Desorption Ionization – Time of Flight Spectrometry (MALDI-TOF). Collected fractions were dried using lyophilization to recover the pure pinholin.

The dry, pure peptide was then spin-labeled with S-(1-oxyl-2,2,5,5-tetramethyl-2,5-dihydro-1H-pyrrol-3-yl)methyl methanesulfonothioate (MTSL), a nitroxide spin label at position Leu25. This position was chosen due to its location in TMD1, and therefore will test our ability to spin label the different conformations adopted by the active $S^{21}68$ and inactive $S^{21}IRS$ pinholin. This was performed by dissolving the pinholin peptide and MTSL, at a $5\times$ molar excess, in DMSO and letting it react while being stirred continuously for 24 h. The reaction was stopped by freezing the solution in liquid nitrogen and then dried using lyophilization.

The resulting crude spin-labeled pinholin was again purified using RP-HPLC and the same two-solvent system on a C4 semi-prep column to remove the excess MTSL. MTSL addition to the pinholin peptide was confirmed through MALDI-TOF mass, as shown in Fig. 3. Collected pure peptide fractions were dried using lyophilization.

2.4. Peptide incorporation into lipid mimetic systems

The pure peptide was incorporated into one of two different lipid mimetic environments, 1,2-Dimyristoyl - sn - Glycero - 3 - Phosphocholine (DMPC)/1,2 - Diheptanoyl - sn - Glycero - 3 - Phosphocholine (DHPC) bicelles, or DMPC multilamellar vesicles (MLV). MLVs are a commonly used mimetic system and have been shown to be successful in mimicking a bilayer for membrane protein studies [20,21]. MLVs were created by mixing the peptide dissolved in 2,2,2-Trifluoroethanol (TFE) with DMPC in chloroform at the desired protein concentration or protein to lipid ratio. Solvents were evaporated off using inert N_2 gas and the remaining lipid/protein film was rehydrated using 4-(2-hydroxyethyl)-1-piperazineethanesulfonic acid (HEPES) buffer at a concentration of 20 mM adjusted to a neutral pH of \sim 7.0. The protein/lipid solution was flash frozen in liquid nitrogen and then sonicated. This process was repeated 3 times to ensure MLV formation.

Active 68-MTSL Active 68-WT 6000 8000 10000 4000 6000 8000 10000 4000 m/z m/z Inactive IRS-MTSL Inactive IRS-WT 4000 6000 8000 10000 4000 6000 8000 10000 m/z m/z

Bicelles were made by taking the dissolved peptide in TFE and adding it to a solution of DMPC and DHPC in chloroform at an optimized q value of 3.6 [22]. Then the solvents were evaporated off using inert $N_2(g)$ and the same process as MLV formation was followed until sample became clear.

2.5. Circular Dichroism

Circular Dichroism (CD) measurements on pinholin were performed on an Aviv Circular Dichroism Spectrometer Model 435 in a quartz cuvette with a 1.0 mm path length. Data was collected from 260 to 190 nm with 1 nm bandwidth at 25 $^{\circ}$ C. CD data was collected on pinholin MLV samples prepared using the conditions outlined in the previous section.

CD spectral simulations and secondary structural content calculations were performed using DICHROWEB software found on http://dichroweb.cryst.bbk.ac.uk [23]. The CDSSTR algorithm was used for all simulations and compared back to reference data set SMP180 with a spectral width of 190–240 nm [24–28]. Molar ellipticity ratios $[\theta]_{222}/[\theta]_{208}$ were calculated to determine the presence of tertiary coiled-coil helices [29,30].

2.6. Continuous wave electron paramagnetic resonance spectroscopy

CW-EPR experiments were performed at the Ohio Advanced EPR Laboratory at Miami University. CW-EPR spectra were collected at X-band on a Bruker EMX EPR spectrometer using an ER041xG microwave bridge and ER4119-HS cavity coupled with a BVT 3000 nitrogen gas temperature controller. Each CW-EPR spectrum was acquired with 42 s field sweep with a central field of 3315 G and sweep width of 100 G, modulation frequency of 100 kHz, modulation amplitude of 1 G, and microwave power of 10 mW at room temperature.

2.7. ³¹P Solid State nuclear magnetic resonance spectroscopy

The ^{31}P solid-state nuclear magnetic resonance measurements were conducted at 25 °C using a Bruker 500 MHz WB UltraShield NMR spectrometer with a 4 mm triple resonance CP-MAS probe. ^{31}P NMR spectra were recorded with ^{1}H decoupling using a 4 μs $\pi/2$ pulse and a 4 s recycle delay, a spectral width of 300 ppm, and by averaging 4 K scans. The free induction decay was processed using 200 Hz of line broadening. All figures were generated using the Igor software package.

Fig. 3. The MALDI-TOF mass spectrum of active (blue) $S^{21}68$ -WT and $S^{21}68$ -L25C-MTSL with a WT m/z of 7546 and MTSL m/z of 7722 and the inactive (red) S^{21} IRS-WT and S^{21} IRS-L25C-MTSL with a WT m/z of 8222 and MTSL m/z of 8397. The shift of +185 comes from the successful coupling of the MTSL to the Cys substituted Leu25 position. The doubly charged ion peaks for all spectra can be seen at one half the target m/z value. (For interpretation of the references to colour in this figure legend, the reader is referred to the Web version of this article.)

3. Results and discussion

This study reports the successful in vitro synthesis of both the active S²¹68 and inactive S²¹IRS forms of the pinholin system using solid phase peptide synthesis (SPPS). The full length active S²¹68 and inactive S²¹IRS forms of the pinholin protein are composed of 68 and 73 amino acids respectively. The optimization of the sample preparation was confirmed through MALDI-TOF spectra that match the predicted molecular weights for each of the wild type pinholins, 7548 Da for the active S²¹68 and 8223 Da for the inactive S²¹IRS (Fig. 1 and 3). A cysteine was substituted into the primary sequence for the leucine at position 25 for future nitroxide spin labeling. After synthesis, the solid phase resin and all amino acid protecting groups were removed in a three-hour reaction using a 30 mL cleavage solution of trifluoroacetic acid (TFA). The resulting peptide was precipitated from solution and washed 3 times using tert-butyl ether. Following the ether washes, the protein was purified using RP-HPLC and fractions were analyzed using MALDI-TOF to confirm the accuracy and overall purity of the synthesis.

3.1. Optimization of the solid phase peptide synthesis

Long hydrophobic peptides are difficult to synthesize, therefore the initial pinholin synthesis was of the first 20 amino acids (see Fig. 1) with each of the following syntheses adding 10 more amino acids to the chain length. The peptide from each synthesis was analyzed using MALDI-TOF to determine which amino acids were not coupling completely. Coupling times and temperatures where adjusted to increase successful coupling as the chain length was extended to the full 73 amino acids of the inactive $\rm S^{21}IRS$ pinholin. Since the pinholin system is naturally cys-less the incorporation of a cysteine at any position along the primary sequence allows for disulfide bond formation to the spin label at specific positions.

The MALDI-TOF results for the synthesis of both the active $S^{21}68$ and inactive $S^{21}IRS$ pinholin wild type using the fourth cleavage condition in the following section can be seen in Fig. 3. The target MW for the active $S^{21}68$ and inactive $S^{21}IRS$ pinholin were 7546 and 8222 Da, respectively. The observed MW from Fig. 3 for the active $S^{21}68$ was found to be 7548 Da while the inactive $S^{21}IRS$ shows a peak at 8223 Da confirming a successful synthesis for both forms of the WT pinholin. Fig. 3 also shows the MALDI-TOF data for the active $S^{21}68$ -L25C-MTSL and inactive $S^{21}IRS$ -L25C-MTSL forms of pinholin. The +185 Da shift in the m/z, 7722 for the active and 8391 for the inactive, confirms the successful spin labeling of both forms of the pinholin. In all cases there is a small peak appearing at one half the target MW corresponding to detection of a doubly charged pinholin ion.

3.2. Optimization of peptide cleavage conditions and HPLC purification

The cleavage protocol was optimized by monitoring the cleavage reaction of various cleavage solutions over time. Four different cleavage conditions were tested based on type and number of certain amino acid side chain protecting groups present [16]. The cleavage conditions for four different solutions are as follows:

Cleavage condition 1 [17] – TFA/EDT/thioanisole/water – 88/5/2/5

Cleavage condition 2 [18] – TFA/phenol/water/thioanisole/EDT – 82.5/5/5/2.5

Cleavage condition 3 [19] – TFA/thioanisole/EDT/anisole – 90/5/3/2

Cleavage condition 4 [17] – TFA/triisoproylsilane/EDT/water – 94/ 1/2.5/2.5

Each of the different components of the cleavage reaction was measured out as a %v/v with a final cleavage solution volume of 30 mL. As each cleavage condition was tested a 5 mL aliquot of the reaction

solution was removed at $t=30,\,60,\,90,\,120,\,150,$ and $180\,\text{min}$. Each aliquot was worked up following the procedure outlined in section 2.2. Finally, each time point was analyzed using MALDI-TOF to confirm the target protein molecular weight.

The MALDI-TOF results clearly identified cleavage condition 4 as the best cleavage condition for this system as it gave the sharpest target peak with the fewest impurity peaks. The MALDI peak at the target molecular weight does not begin to appear until an hour after the reaction begins. The MALDI results show no change in peak shape between the 2.5 and 3 h aliquots indicating the completion of the cleavage reaction.

3.3. Optimization of MALDI-TOF sample conditions and matrix

To optimize the MALDI-TOF analysis the pinholin peptide was dissolved in solutions of increasing amounts of acetonitrile in water. Each solution was spotted using one of three different matrices at a 1:1 ratio, α -Cyano-4-hydroxycinnamic acid (CHCA) matrix, 2,5-Dihydroxybenzoic acid (DHB) matrix, and Sinapic Acid (SA) matrix. The sample condition of 85% acetonitrile spotted with sinapic acid matrix gave the clearest resolution of MS peaks. Closer analysis of MALDI-TOF results revealed peaks at a higher m/z ratio indicating the presence of unremoved protecting groups during cleavage step. This process lead to the optimization of the cleavage reaction to remove these protecting groups.

3.4. Circular Dichroism of active S²¹68 and inactive S²¹IRS pinholin

CD spectroscopy is primarily used in the biochemical field to determine the global secondary structure of large macromolecules, such as peptides and proteins. This is accomplished through measuring the difference in absorption between left and right-handed circularly polarized light over a range of wavelengths [31]. The folding of the protein into a helical secondary structure was confirmed for both the active S²¹68 and inactive S²¹IRS pinholin using CD spectroscopy.

CD samples for both the active S2168 and inactive S21IRS forms of wild type pinholin were separately prepared in DMPC MLVs at a protein to lipid ratio of 1:500 with a final concentration of protein equal to 50 μM. Background scattering at lower wavelengths was minimized by subtracting the data collected from empty DMPC MLVs run at the same lipid concentration from the protein sample in DMPC MLVs. The resulting CD spectra of the active S²¹68 pinholin (blue) and the inactive S²¹IRS (red) are shown in Fig. 4. Both forms of pinholin show a predominately helical structure with double minima at 208 nm and 222 nm and a large positive peak at 195 nm. The active S²¹68 pinholin showed a calculated helical content of 83%, while the inactive S²¹IRS pinholin secondary structure calculation determined 82% helical content. The percent normalized RMSD value calculated for both forms of the pinholin were less than 1.0% [28]. The helical content agrees well to the expected secondary structure of the protein based on previous studies in the literature [11].

To give a more in-depth analysis of the CD spectra the molar ellipticity ratio of $[\theta]_{222}/[\theta]_{208}$ was calculated for both forms of the pinholin. A molar ellipticity ratio exceeding a value of 1 is indicative of coiled-coil helical structures [29,30,32]. The molar ellipticity ratio $[\theta]_{222}/[\theta]_{208}$ for both forms of the pinholin was found to be 1.4 and therefore, this coiled-coil structure was determined to be present for both the active $S^{21}68$ and inactive $S^{21}IRS$ forms. This matches with the current predicted pinholin lysis pathway in which the pinholin begin to oligomerize, forming more coiled-coils, as more pinholin proteins accumulate in the membrane ultimately resulting in the lysis of the membrane [11,15]. Further evidence of this will be shown in future experiments in which the oligomerization state of pinholin will be investigated as a function of concentration.

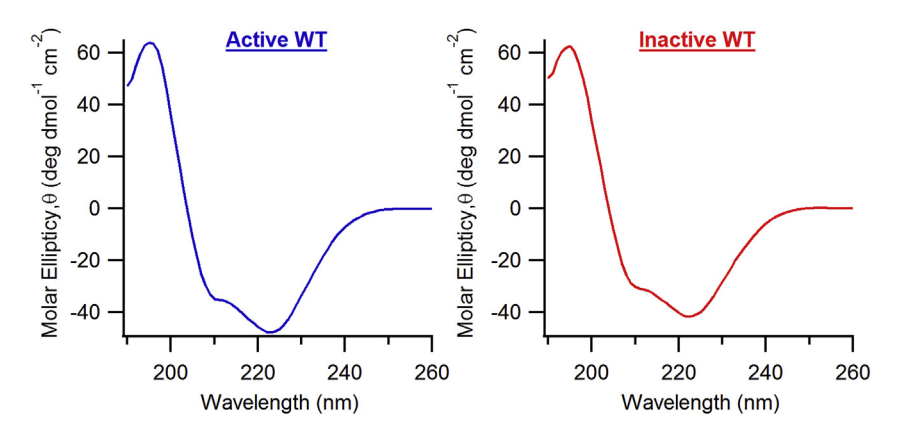


Fig. 4. Circular Dichroism spectra of both the active S²¹68 (blue) and inactive S²¹IRS (red) forms of the pinholin protein in DMPC MLVs showing local minima at 208 and 222 nm with a large positive peak at 195 nm, indicative of alpha helical secondary structure. (For interpretation of the references to colour in this figure legend, the reader is referred to the Web version of this article.)

3.5. Continuous wave EPR measurements of pinholin

CW-EPR spectroscopy can be used to probe the dynamic and structural properties of both solution and membrane proteins. CW-EPR spectroscopy of these spin-labeled molecules can reveal information about the motion of the nitroxide side chain, solvent accessibility, and the polarity of the surrounding environment [21,33].

The successful spin labeling of the pinholin protein and incorporation into both bicelle and MLV lipid mimetic systems is shown in the CW-EPR spectra in Fig. 5. This EPR data was also used to calculate spin labeling efficiency for each peptide which ranged from ${\sim}85$ to 90%

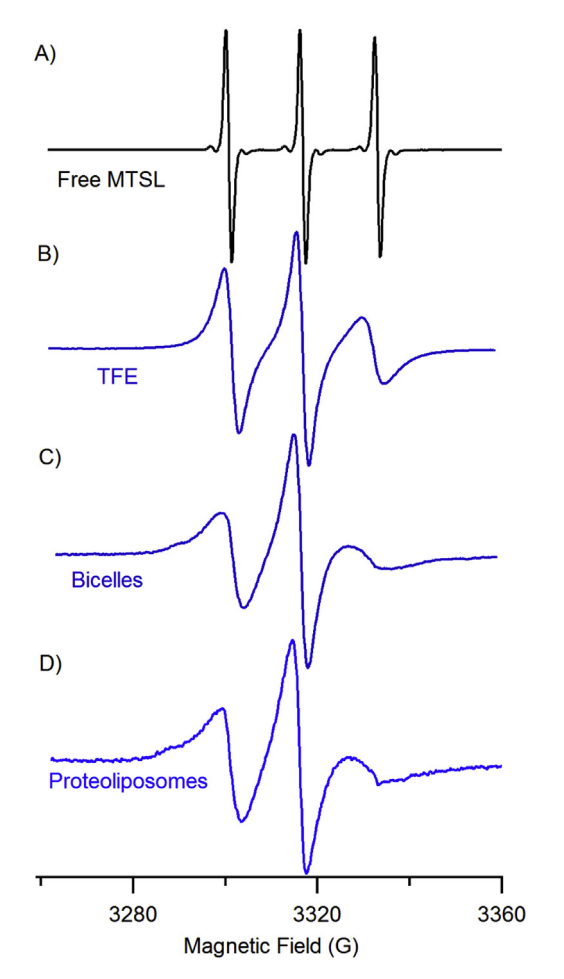


Fig. 5. CW-EPR spectra of A) free MTSL at 300 μ M in water B) MTSL coupled to the active S²¹68 pinholin protein at Leu25 dissolved in TFE C) MTSL labeled pinholin incorporated into 1:500 DMPC/DHPC bicelles and D) MTSL labeled pinholin incorporated into 1:500 DMPC MLVs.

labeling efficiency. The EPR spectra for unbound nitroxide spin labels typically consist of three sharp peaks of relatively similar intensities, as seen in Fig. 5A. Upon binding to a protein, such as pinholin, the MTSL will have a more restricted mobility due to the presence of the protein backbone. This decrease in the motion of the MTSL will broaden the lines in the EPR spectra and cause a decrease in their amplitude which is present in Fig. 5B [33,34]. The broadening of the EPR spectral linewidth is quantitatively determined by measuring the central line width. In Fig. 5A the free MTSL spectra shows a central line width of 1.4 G, while the MTSL bound to the pinholin, 5B, has a central line width of 2.9 G. The line broadening of the EPR spectra from Fig. 5A and B confirms the successful disulfide bond formation between the free MTSL and the Cys side chain of the pinholin due to a more restricted environment for the bound SL.

Incorporation of the pinholin into a lipid mimetic system should restrict the motion of the spin label even further through interactions with the lipid's hydrocarbon acyl chains. Since the broadening of the EPR spectra is proportional to the mobility of the spin label, the EPR spectra from pinholin incorporated into bicelles and MLVs show a greater degree of broadening than the labeled protein in solution (TFE) as seen when comparing Fig. 5B to C, D. The central line widths of pinholin in bicelles versus pinholin in MLVs are 3.2 G and 3.3 G, respectively. The similarity of the central line width between the lipid incorporated samples is due to the similarity of the local environment around the spin label. Both bicelles and MLVs are good mimetics for lipid bilayers as opposed to a mimetic like micelles, which only mimic the hydrophobic environment of the membrane but cannot recreate the conditions of a bilayer. Therefore, the local environment and acyl chain packing around the spin label for both bicelles and MLVs will be similar in either mimetic.

3.6. ³¹P Solid State – NMR spectroscopy of pinholin

Solid State NMR spectroscopy is a powerful biophysical technique which utilizes the presence of directionally dependent anisotropic interactions to probe the dynamics or kinetics of a system, specifically the membrane system for this study [35]. ³¹P SS-NMR experiments were used to measure the chemical shift anisotropy (CSA) of the phosphorus head groups of DMPC lipids [20]. The degree in which the pinholin interacts with the ³¹P lipid head group will help to probe the differences between the roles of the active S²¹68 and inactive S²¹IRS forms of the pinholin in the lytic pathway from the perspective of the membrane.

 $^{31}\mathrm{P}$ SS-NMR samples were prepared using the wild type active $S^{21}68$ and inactive $S^{21}\mathrm{IRS}$ forms of the pinholin incorporated into DMPC MLVs at 1 mol%. More protein is required here to account for the lower sensitivity of NMR when compared to EPR spectroscopy. Empty DMPC MLVs, active $S^{21}68$ pinholin in DMPC MLVs, and inactive $S^{21}\mathrm{IRS}$ pinholin in DMPC MLVs at 25 °C are shown in Fig. 6A, B, and C, respectively. The shape of the static $^{31}\mathrm{P}$ SS-NMR spectra for the empty MLVs, active $S^{21}68$, and inactive $S^{21}\mathrm{IRS}$ are characteristic of lamellar phase

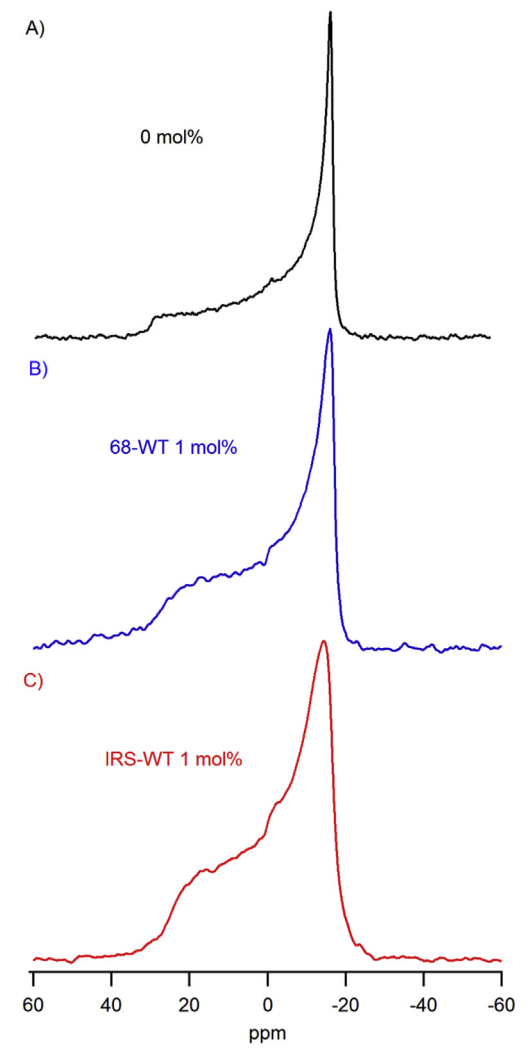


Fig. 6. Static 31 P solid-state NMR spectrum of: A) empty DMPC MLVs (black). B) 1mol% active S 21 68-WT pinholin in DMPC MLVs (blue). C) 1mol% inactive IRS-WT pinholin in DMPC MLVs (red). (For interpretation of the references to colour in this figure legend, the reader is referred to the Web version of this article.)

lipid mimetics and show axial symmetry. The CSA width for each of the NMR spectra were found to be 48.0 ppm for empty DMPC MLVs, 44.7 ppm for active $S^{21}68$ pinholin incorporated in DMPC MLVs, and 42.2 ppm for the inactive $S^{21}IRS$ pinholin incorporated in DMPC MLVs. The smaller CSA width for both the active $S^{21}68$ and inactive $S^{21}IRS$ pinholin when compared to the empty MLVs confirms the interaction of the protein with the lipid mimetic system. The absence of an isotropic peak suggests the integrity of the MLV mimetic system is not compromised with the addition of the pinholin protein. The smaller CSA for the inactive $S^{21}IRS$ pinholin (42.2 ppm) indicates the inactive form is influencing the ^{31}P DMPC lipid head groups more than the active $S^{21}68$ form. These differences suggest that the active $S^{21}68$ and inactive $S^{21}IRS$ pinholins behave differently once incorporated into the lipid bilayer. This difference will be further explored in future studies using both ^{31}P T₁ measurements and ^{2}H lipid acyl chain experiments.

4. Conclusion

In this study we report the synthesis of both the active $S^{21}68$ and inactive $S^{21}IRS$ forms of the pinholin protein using solid phase peptide synthesis. The measured CD data of both forms of the pinholin, matched the predicted alpha helical content. The CD molar ellipticity ratio also

provided preliminary data of the helical packing required of the pinholin to attain functionality and will be explored to a greater extent in future works. CW-EPR spectroscopy was used to successfully show spin labeling of the pinholin as well as incorporation into both bicelles and MLV lipid mimetic systems. The success of this measurement opens the door for more in depth EPR structural and dynamic studies to be conducted in the future, such as pulsed EPR measurements [36-40]. ³¹P SS-NMR spectroscopy allowed for the study of the pinholin system from the lipid perspective and showed interactions of both forms of the pinholin with the lipid membrane, to varying degrees, through decreases in the CSA width when compared to the empty DMPC MLVs. These differences in the way the active S²¹68 and inactive S²¹IRS forms of the pinholin interact with the membrane suggest differences in the externalization of TMD1, and ultimately the role each form plays in the bacteriophage lytic pathway. Additionally, ³¹P T₁ relaxation time measurements and ²H NMR experiments can be conducted to further probe the interaction of the pinholin with the acyl chain and lipid head groups to better understand how S2168 and S21IRS differ in their membrane interaction.

Declarations of interest

None.

Acknowledgments

We would like to thank members of the Young group at Texas A&M University for their enthusiasm in the continued pinholin work as well as their experimental suggestions. This work was generously supported by a NSF CHE-1807131 grant and a NIGMS/NIH Maximizing Investigator's Research Award (MIRA) R35 GM126935 award. Gary A. Lorigan would also like to acknowledge support from the John W. Steube Professorship.

Appendix A. Supplementary data

Supplementary data to this article can be found online at https://doi.org/10.1016/j.ab.2018.12.003.

References

- R. Young, I. Wang, Phage Lysis. The Bacteriophages, second ed. ed., Oxford Univ Press, Oxford, 2006.
- [2] R. Young, Phage Lysis: do we have the hole story yet? Curr. Opin. Microbiol. 16 (2013) 1–8.
- [3] R. Young, Phage lysis: three steps, three choices, one outcome, J. Microbiol. 52 (2014) 243–258.
- [4] R. Young, I.N. Wang, W.D. Roof, Phages will out: strategies of host cell lysis, Trends Microbiol. 8 (2000) 120–128.
- [5] R. Young, Bacteriophage holins: deadly diversity, J. Mol. Microbiol. Biotechnol. 4 (2002) 21–36.
- [6] T. Park, D.K. Struck, C.A. Dankenbring, R. Young, The pinholin of lambdoid phage 21: control of lysis by membrane depolarization, J. Bacteriol. 189 (2007) 9135–9139.
- [7] M. Xu, D.K. Struck, J. Deaton, I.N. Wang, R. Young, A signal-arrest-release sequence mediates export and control of the phage P1 endolysin, Proc. Natl. Acad. Sci. U. S. A. 101 (2004) 6415–6420.
- [8] J.H. Grose, S.R. Casjens, Understanding the enormous diversity of bacteriophages: the tailed phages that infect the bacterial family enterobacteriaceae, Virology 468 (2014) 421–443.
- [9] M. Barenboim, C.Y. Chang, F.D. Hajj, R. Young, Characterization of the dual start motif of a class II holin gene, Mol. Microbiol. 32 (1999) 715–727.
- [10] M.T. Bonovich, R. Young, Dual start motif in 2 lambdoid s-genes unrelated to lambda-s, J. Bacteriol. 173 (1991) 2897–2905.
- [11] T. Pang, C.G. Savva, K.G. Fleming, D.K. Struck, R. Young, Structure of the lethal phage pinholin, Proc. Natl. Acad. Sci. Unit. States Am. 106 (2009) 18966–18971.
- [12] T. Pang, T. Park, R. Young, Mutational analysis of the S21 pinholin, Mol. Microbiol. 76 (2010) 68–77.
- [13] T. Park, D.K. Struck, J.F. Deaton, R. Young, Topological dynamics of holins in programmed bacterial lysis, Proc. Natl. Acad. Sci. U. S. A. 103 (2006) 19713–19718.
- [14] T. Pang, T. Park, R. Young, Mapping the pinhole formation pathway of S21, Mol. Microbiol. 78 (2010) 710–719.

- [15] T. Pang, T.C. Fleming, K. Pogliano, R. Young, Visualization of pinholin lesions in vivo, Proc. Natl. Acad. Sci. U. S. A. 110 (2013) E2054–E2063.
- [16] P.R. Hansen, A. Oddo, Fmoc solid-phase peptide synthesis, peptide antibodies, Methods and Protocols 1348 (2015) 33–50.
- [17] P. Lloyd-Williams, F. Albericio, E. Giralt, Chemical Approaches to the Synthesis of Peptides and Proteins, CRC Press, 1997.
- [18] D.S. King, C.G. Fields, G.B. Fields, A cleavage method which minimizes side reactions following fmoc solid-phase peptide-synthesis, Int. J. Pept. Protein Res. 36 (1990) 255–266.
- [19] F. Albericio, N. Kneibcordonier, S. Biancalana, L. Gera, R.I. Masada, D. Hudson, G. Barany, Preparation and application of the 5-(4-(9-Fluorenylmethyloxycarbonyl)Aminomethyl-3,5-Dimethoxyphenoxy)Vale ric acid (pal) handle for the solid-phase synthesis of C-terminal peptide amides under mild conditions, J. Org. Chem. 55 (1990) 3730–3743.
- [20] S. Abu-Baker, G.A. Lorigan, Phospholamban and its phosphorylated form interact differently with lipid bilayers: a (31)P, (2)H, and (13)C solid-state NMR spectroscopic study, Biochemistry 45 (2006) 13312–13322.
- [21] I.D. Sahu, R.M. McCarrick, G.A. Lorigan, Use of electron paramagnetic resonance to solve biochemical problems, Biochemistry 52 (2013) 5967–5984.
- [22] T.B. Cardon, E.K. Tiburu, G.A. Lorigan, Magnetically aligned phospholipid bilayers in weak magnetic fields: optimization, mechanism, and advantages for X-band EPR studies, J. Magn. Reson. 161 (2003) 77–90.
- [23] L. Whitmore, B.A. Wallace, Protein secondary structure analyses from circular dichroism spectroscopy: methods and reference databases, Biopolymers 89 (2008) 392–400.
- [24] A. Abdul-Gader, A.J. Miles, B.A. Wallace, A reference dataset for the analyses of membrane protein secondary structures and transmembrane residues using circular dichroism spectroscopy, Bioinformatics 27 (2011) 1630–1636.
- [25] L.A. Compton, W.C. Johnson, Analysis of protein circular-dichroism spectra for secondary structure using a simple matrix multiplication, Anal. Biochem. 155 (1986) 155–167.
- [26] P. Manavalan, W.C. Johnson, Variable selection method improves the prediction of protein secondary structure from circular-dichroism spectra, Anal. Biochem. 167 (1987) 76–85.
- [27] N. Sreerama, R.W. Woody, Estimation of protein secondary structure from circular dichroism spectra: comparison of CONTIN, SELCON, and CDSSTR methods with an expanded reference set. Anal. Biochem. 287 (2000) 252–260.

- [28] D. Mao, E. Wachter, B.A. Wallace, Folding of the mitochondrial proton adenosinetriphosphatase proteolipid channel in phospholipid-vesicles, Biochemistry 21 (1982) 4960–4968.
- [29] J. Liu, Y. Zheng, C.-S. Cheng, N.R. Kallenbach, M. Lu, A seven-helix coiled coil, Proc. Natl. Acad. Sci. Unit. States Am. 103 (2006) 15457–15462.
- [30] N.E. Zhou, C.M. Kay, R.S. Hodges, Synthetic model proteins positional effects of interchain hydrophobic interactions on stability of 2-stranded alpha-helical coiledcoils, J. Biol. Chem. 267 (1992) 2664–2670.
- [31] S.M. Kelly, T.J. Jess, N.C. Price, How to study proteins by circular dichroism, Biochim. Biophys. Acta Protein Proteonomics 1751 (2005) 119–139.
- [32] T.T. Zheng, A. Boyle, H.R. Marsden, D. Valdink, G. Martelli, J. Raap, A. Kros, Probing coiled-coil assembly by paramagnetic NMR spectroscopy, Org. Biomol. Chem. 13 (2015) 1159–1168.
- [33] I.D. Sahu, G.A. Lorigan, Site-directed spin labeling EPR for studying membrane proteins, BioMed Res. Int. (2018) 3248289.
- [34] I.D. Sahu, A.F. Craig, M.M. Dunagan, K.R. Troxel, R.F. Zhang, A.G. Meiberg, C.N. Harmon, R.M. McCarrick, B.M. Kroncke, C.R. Sanders, G.A. Lorigan, Probing structural dynamics and topology of the KCNE1 membrane protein in lipid bilayers via site-directed spin labeling and electron paramagnetic resonance spectroscopy, Biochemistry 54 (2015) 6402–6412.
- [35] T.R. Molugu, S. Lee, M.F. Brown, Concepts and methods of solid-state NMR spectroscopy applied to biomembranes, Chem. Rev. 117 (2017) 12087–12132.
- [36] I.D. Sahu, B.M. Kroncke, R.F. Zhang, M.M. Dunagan, H.J. Smith, A. Craig, R.M. McCarrick, C.R. Sanders, G.A. Lorigan, Structural investigation of the transmembrane domain of KCNE1 in proteoliposomes, Biochemistry 53 (2014) 6392–6401.
- [37] E.F. Vincent, I.D. Sahu, A.J. Costa-Filho, E.M. Chilli, G.A. Lorigan, Conformational changes of the HsDHODH N-terminal microdomain via DEER spectroscopy, J. Phys. Chem. B 119 (2015) 8693–8697.
- [38] L.S. Liu, G. Lorigan, Probing the secondary structure of membrane proteins with the pulsed EPR ESEEM technique, Biophys. J. 106 (2014) 192A-192A.
- [39] L.S. Liu, I.D. Sahu, L. Bottorf, R.M. McCarrick, G.A. Lorigan, Investigating the secondary structure of membrane peptides utilizing multiple H-2-Labeled hydrophobic amino acids via electron spin echo envelope modulation (ESEEM) spectroscopy, J. Phys. Chem. B 122 (2018) 4388–4396.
- [40] G.A. Lorigan, Probing the structure of membrane proteins with ESEEM and DEER pulsed EPR techniques, Biophys. J. 102 (2012) 423A-423A.